International Journal of Multiphase Flow 36 (2010) 549–557

Contents lists available at ScienceDirect

International Journal of Multiphase Flow

journal homepage: www.elsevier.com/locate/ijmulflow

Flooding in two-phase counter-current flows: Numerical investigation of the gas–liquid wavy interface using the Navier–Stokes equations

Yu.Ya. Trifonov *

Institute of Thermophysics, Siberian Branch of Russian Academy of Sciences, Novosibirsk 630090, Russia

ARTICLE INFO

Article history:
Received 16 August 2009
Received in revised form 18 December 2009
Accepted 15 March 2010
Available online 23 March 2010

Keywords:
Viscous liquid film flow
Nonlinear waves
Counter-current gas liquid flow
Flooding

ABSTRACT

This paper is devoted to a theoretical analysis of counter-current gas–liquid wavy film flow between vertical plates. We consider two-dimensional nonlinear waves on the interface over a wide variation of parameters. We use the Navier–Stokes equations in their full statement to describe the liquid phase hydrodynamics. For the gas phase equations, we use the Benjamin-Miles approach where the liquid phase is a small disturbance for the turbulent gas flow. We find a region of the superficial velocity where we have two solutions at one set of the problem parameters and where the flooding takes place. We calculate the flooding dependences on the gas/liquid physical properties, on the liquid Reynolds number and on the distance between the plates. These computations allow us to present the correlation for the onset of flooding that based on the fundamental equations and principles.

1. Introduction

Theoretical studies of film flows began with the classical work of Nusselt (1916), where he obtained exact solution of the Navier–Stokes equations for a thin viscous layer falling down a smooth vertical wall. The pioneering works of Kapitza (1948) and Kapitza and Kapitza (1949) followed this where they considered both experimentally and theoretically the different wavy flow regimes both in the presence and absence of interfacial shear. There are many theoretical and experimental papers devoted to the nonlinear waves on the surface of a free-falling liquid film (see, for example, Jones and Whitaker, 1966; Chu and Dukler, 1974; Alekseenko et al., 1985; Joo et al., 1991; Liu et al., 1993; Lee and Mei, 1996) where a complicated structure of the wavy film flow was revealed. We mention here some of the features: (a) the existence of both spatial and temporal evolution of the film flow; (b) the transition of two-dimensional waves into three-dimensional structures; and (c) the existence of qualitatively different film flow regimes. Interfacial shear for a counter-current liquid–gas flow gives an additional interesting and technically important phenomenon – flooding. Semenov (1944) was the first who observed this phenomenon experimentally. Thin layer of water falls down as a film inside the glass vertical tube of $D = 8$, 13.8 and 22 mm in the experiments. The counter-current air velocity increases from 0 m/s and up to 35 m/s. He concluded that below the air velocity of 3–3.5 m/s (for tube of $D = 13.8$ mm), the gas flow had no effect on the liquid film wavy structure. Above the air velocity 4 m/s, the waves amplitude increased and at 7.3 m/s (for $D = 13.8$ mm), he observed flooding. A great number of works have been devoted to the prediction of the flooding for different liquids and gases and for different channels. There are many correlations in the literature to explain the flooding where the liquid changes direction (see, for example, the reviews by Dukler and Smith (1977), Tien and Liu (1979), Drosos et al. (2006)). The general problem is that "the correlations are unable to predict flooding under conditions significantly different from the ones used to construct the correlations in the first place" (Maron and Dukler, 1984; Zapke and Kröger, 2000b). Most of the papers devoted to flooding are experimental measurements and observations. We mention here some of the experiments in vertical rectangular channels. Lee and Bankoff (1984) conducted flooding experiments in a rectangular channel using steam-water counter-current flow. They indicated the significant effect of the channel gap on flooding. Biage and Delhaye (1989) studied the case of air–water flow in a wide vertical channel with a relatively large gap. They showed that the onset of flooding is associated with droplet entrainment. Zapke and Kröger (2000a,b) studied the dependence of flooding on duct geometry and on gas/liquid physical properties. They used water, methanol, propanol, air, argon, helium and hydrogen as working fluids and demonstrated that the flooding gas velocity was strongly dependent on duct height and fluid densities. They discussed a validity of different flooding correlations and suggested new equation to correlate their data based on the Froude and Ohnesorge numbers. Vlachos et al. (2001) reported flooding data obtained in a vertical rectangular channel with 5 and 10 mm gap. Sudo (1996) carried

* Tel.: +7 383 330 60 40; fax: +7 383 330 84 80.
E-mail address: trifonov@itp.nsc.ru

0301-9322/$ - see front matter © 2010 Elsevier Ltd. All rights reserved.
doi:10.1016/j.ijmultiphaseflow.2010.03.006

out experiments in channels with gap and width 2.3–12.3 mm and 33–66 mm, respectively, and reported that the role of channel gap is very important. Drosos et al. (2006) reported data obtained in a vertical channel with 10 mm gap using air and three liquids (water, 1.5% and 2.5% aqueous butanol solutions). They presented results of visual observations, instantaneous local film thickness data, and shear stress data obtained by use of an electrochemical technique. The onset of flooding in their experiments was defined as "the condition where at least part of the liquid flow is reversed in direction and carried above the liquid entrance section, even in the form of droplets" (Hewitt, 1995). For the air/water system they measured the onset of flooding around 8–12 m/s, depending on the value of Re, and demonstrated that the superficial gas velocity at the onset of flooding decreases with the liquid Reynolds number increasing.

There are only a few theoretical works where the counter-current gas–liquid flow with a wavy interface is considered. Demekhin et al. (1989), using integral equations for the liquid phase, considered the gas turbulent flow as "pseudo-laminar" (Benjamin, 1959; Miles, 1957) to obtain the gas reaction to the liquid hydrodynamics. They computed the t-evolution of the initial x-periodical disturbances of the film thickness at different values of the nondimensional shear. At some value of the shear stress, they observed a dramatic increasing of the disturbances amplitude during the time evolution. The averaged film thickness is held constant in their calculations and the averaged liquid flow rate varies during the time-evolution.

The goal of the present work is to study different steady-state traveling regimes of counter-current gas–liquid film flow. To define the flooding onset quantitatively, we need to analyze the wave structure changes when the problem parameters will be close to the critical parameters measured experimentally. A theoretical model for the onset of flooding provides the capability to analyze the flooding dependence on channel geometry and on liquid/gas physical properties. The averaged liquid flow rate is held constant in present calculations of nonlinear waves, which is important feature of the obtained results. The onset of flooding is a limiting factor in the operation of various types of devices used by the chemical industry (for example, two-phase plate heat exchangers and compact reflux condensers). The flooding prediction will be interesting for many applications.

2. Governing equations

Using a rectangular coordinate system, the Navier–Stokes equations with the corresponding boundary conditions describe the counter-current gas–liquid wavy film flow between vertical plates (see Fig. 1). We consider the liquid wavy film flow as a small disturbance for the turbulent gas flow between the plates. In this case, the gas velocities and pressure have form $u^g = u_b^g + \hat{u}^g$, $v^g = \hat{v}^g$, $P^g = P_b^g + \hat{P}^g$, where the $u_b^g(y)$, $P_b^g(x)$ correspond to a basic solution of the turbulent gas flow through a smooth channel and the values $\hat{u}^g(x,t,y)$, $\hat{v}^g(x,t,y)$, $\hat{P}^g(x,t,y)$ correspond to the gas flow perturbations due to the thin liquid film falling down the channel wall. The liquid phase governing equations, the boundary conditions on the wall and along the interface, the linearization of the gas phase equations near the basic solution and the symmetry conditions along the channel middle are as follows:

$$\frac{\partial u}{\partial t} + u\frac{\partial u}{\partial x} + v\frac{\partial u}{\partial y} = -\frac{\partial P}{\partial x} - \varepsilon_\rho n^2 \frac{dP_b^g}{dx} + \frac{1}{\varepsilon \mathrm{Re}}\left(3 + \frac{\partial^2 u}{\partial y^2} + \varepsilon^2 \frac{\partial^2 u}{\partial x^2}\right); \tag{1}$$

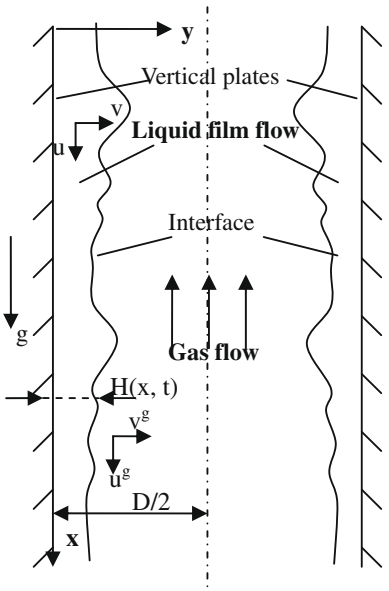

Fig. 1. Scheme of counter-current gas/liquid flow.

$$\varepsilon^2\left(\frac{\partial v}{\partial t} + u\frac{\partial v}{\partial x} + v\frac{\partial v}{\partial y}\right) = -\frac{\partial P}{\partial y} + \frac{\varepsilon}{\mathrm{Re}}\left(\frac{\partial^2 v}{\partial y^2} + \varepsilon^2 \frac{\partial^2 v}{\partial x^2}\right);$$

$$\frac{\partial u}{\partial x} + \frac{\partial v}{\partial y} = 0; \tag{2), (3}$$

$$u = v = 0, \quad y = 0; \quad v = \frac{\partial H}{\partial t} + u\frac{\partial H}{\partial x}, \quad y = H(x,t); \tag{4), (5}$$

$$(\sigma_{ik}^g - \sigma_{ik})n_k\tau_i = 0 \Rightarrow \varepsilon_\mu n\left(\frac{du_b^g}{dy} + \frac{d^2u_b^g}{dy^2}H + \frac{\partial \hat{u}^g}{\partial y} + 4\varepsilon^2\frac{\partial \hat{v}^g}{\partial y}\frac{\partial H}{\partial x}\frac{1}{1-\varepsilon^2\left(\frac{\partial H}{\partial x}\right)^2}\right)\Bigg|_{y=0} - \left(\frac{\partial u}{\partial y} + \varepsilon^2\frac{\partial v}{\partial x} + 4\varepsilon^2\frac{\partial v}{\partial y}\frac{\partial H}{\partial x}\frac{1}{1-\varepsilon^2\left(\frac{\partial H}{\partial x}\right)^2}\right)\Bigg|_{y=H(x,t)} = 0; \tag{6}$$

$$(\sigma_{ik}^g - \sigma_{ik})n_k n_i - \frac{\sigma}{R} = 0 \Rightarrow \left(-\varepsilon_\rho n^2\hat{P}^g + \frac{2\varepsilon\varepsilon_\mu n}{\mathrm{Re}}\frac{\partial \hat{v}^g}{\partial y}\frac{1+\varepsilon^2\left(\frac{\partial H}{\partial x}\right)^2}{1-\varepsilon^2\left(\frac{\partial H}{\partial x}\right)^2}\right)\Bigg|_{y=0} + \left(P - \frac{2\varepsilon}{\mathrm{Re}}\frac{\partial v}{\partial y}\frac{1+\varepsilon^2\left(\frac{\partial H}{\partial x}\right)^2}{1-\varepsilon^2\left(\frac{\partial H}{\partial x}\right)^2}\right)\Bigg|_{y=H(x,t)} + \frac{(3Fi)^{1/3}}{\mathrm{Re}^{5/3}}\frac{\varepsilon^2\frac{\partial^2 H}{\partial x^2}}{\left[1+\varepsilon^2\left(\frac{\partial H}{\partial x}\right)^2\right]^{3/2}} = 0; \tag{7}$$

$$\left(\frac{du_b^g}{dy}H + \hat{u}^g\right)\Big|_{y=0} = \frac{1}{n}u|_{y=H(x,t)}, \quad \hat{v}^g|_{y=0} = \frac{1}{n}v|_{y=H(x,t)}; \tag{8}$$

$$\frac{1}{n}\frac{\partial \hat{u}^g}{\partial t} + u_b^g\frac{\partial \hat{u}^g}{\partial x} + \hat{v}^g\frac{du_b^g}{dy} = -\frac{\partial \hat{P}^g}{\partial x} + \frac{1}{\varepsilon\varepsilon_2\mathrm{Re}^g}\left(\frac{\partial^2 \hat{u}^g}{\partial y^2} + \varepsilon^2\frac{\partial^2 \hat{u}^g}{\partial x^2}\right); \tag{9}$$

$$\varepsilon^2\left(\frac{1}{n}\frac{\partial \hat{v}^g}{\partial t} + u_b^g\frac{\partial \hat{v}^g}{\partial x}\right) = -\frac{\partial \hat{P}^g}{\partial y} + \frac{\varepsilon}{\varepsilon_2\mathrm{Re}^g}\left(\frac{\partial^2 \hat{v}^g}{\partial y^2} + \varepsilon^2\frac{\partial^2 \hat{v}^g}{\partial x^2}\right); \tag{10}$$

$$\frac{\partial \hat{u}^g}{\partial x} + \frac{\partial \hat{v}^g}{\partial y} = 0; \tag{11}$$

$$\frac{\partial \hat{u}^g}{\partial y} = 0, \quad \hat{v}^g = 0, \quad y = \frac{1}{2\varepsilon_2}. \tag{12}$$

Here u is the liquid velocity component in the gravity direction, v is the liquid velocity in the y-direction, P is the pressure in the liquid, σ_{ik} is the stress tensor components in liquid, and $H(x, t)$ is the instantaneous local film thickness. The stress tensor components in gas are σ^g_{ik}, $\boldsymbol{n_k}$ and $\boldsymbol{\tau_i}$ are the components of normal and tangential unit vectors to the interface, respectively. The interface curvature radius is R and we assume summing over repeated indexes in the boundary conditions.

Eqs. (1)–(12) are in a nondimensional form and we used scales as follows (asterisk denotes the dimensional variables):

$$x = \frac{x^*}{L}; \quad t = \frac{u_0 t^*}{L}; \quad y = \frac{y^*}{H_0}; \quad u = \frac{u^*}{u_0}; \quad v = \frac{v^*}{\varepsilon u_0}; \quad P = \frac{P^*}{\rho u_0^2};$$
$$H = \frac{H^*}{H_0}; \quad u^g = \frac{(u^g)^*}{u_0^g}; \quad v^g = \frac{(v^g)^*}{\varepsilon u_0^g}; \quad P^g = \frac{(P^g)^*}{\rho_g (u_0^g)^2};$$
$$\mathrm{Re} \equiv \frac{u_0 H_0}{\nu} \equiv \frac{g(1-\varepsilon_\rho)H_0^3}{3\nu^2}; \quad \varepsilon = \frac{H_0}{L}; \quad \varepsilon_2 = \frac{H_0}{D}; \quad \varepsilon_\mu = \frac{\mu_g}{\mu};$$
$$\varepsilon_\rho = \frac{\rho_g}{\rho}; \quad n = \frac{u_0^g}{u_0}; \quad \mathrm{Re}^g = \frac{u_0^g D}{\nu_g}; \quad Fi = \frac{(\sigma/\rho)^3}{g(1-\varepsilon_\rho)\nu^4}.$$

Here ν, μ is the liquid kinematic and dynamic viscosity, respectively, ρ is the liquid density, σ is the surface tension. The wave period is L, Fi is the film number, H_0 and u_0 is the Nusselt's film thickness and velocity, respectively. The liquid Reynolds number is $\mathrm{Re} = U_{LS} D_e / 4\nu$, where $U_{LS} = Q_L/S$ is the liquid superficial velocity, $D_e = 4S/p$ is the equivalent hydraulic diameter ($D_e = 2D$), p is the channel wetted perimeter, Q_L is the volumetric liquid flow rate supplied per the channel cross-section S, D is the distance between the vertical plates. The gas kinematic and dynamic viscosities are ν_g, μ_g, respectively, ρ_g is the gas density, Re^g is the gas Reynolds number and u_0^g is a half of the gas superficial velocity U_{GS} ($u_0^g = 0.5U_{GS} = 0.5Q_G/S$, Q_G is the volumetric gas flow rate supplied per the channel cross-section).

Eqs. (1) and (2) and (9) and (10) represent the momentum conservation for the liquid and gas phase, respectively. We use the mean-velocity profiles $u_b^g(y)$ and $\hat{u}^g(x,t,y)$ for both the basic and disturbed turbulent gas flow. The gas phase pulsations generated by the wavy film surface are small and we omit them in Eqs. (9) and (10). Miles (1957) and Benjamin (1959) were the first who considered the turbulent gas flow over a wavy boundary and who formulated the "quasi-laminar" approach. Eqs. (3) and (11) is the mass conservation law for the liquid and gas, correspondingly. Eqs. (4) and (8) are the no-slip conditions on the plate and on the interface, respectively. Eq. (5) is a kinematic condition along the interface. Eqs. (6) and (7) formulate the tangential and normal stress equilibrium along the interface, correspondingly. We suggest that the wavy film surface is a small disturbance for the gas turbulent flow and use an expansion of the gas phase boundary conditions in Eqs. (6)–(8). There is a symmetry of the two-phase flow with respect to the channel middle and Eq. (12) is the symmetry condition.

Further, we consider the steady-state traveling solutions of Eqs. (1)–(12) – $\left[H(x_1), u(x_1,y), v(x_1,y), P(x_1,y), \hat{u}^g(x_1,y), \hat{v}^g(x_1,y), \hat{P}^g(x_1,y)\right]$, $x_1 \equiv x - ct$, $\boldsymbol{c}$ is the wave phase velocity. We suggest that the gas superficial velocity is much high than the liquid film velocity, $n \gg 1$. In this case, we neglect terms $\frac{1}{n}\frac{\partial \hat{u}^g}{\partial t} = -\frac{c}{n}\frac{\partial \hat{u}^g}{\partial x_1}$ and $\frac{1}{n}\frac{\partial \hat{v}^g}{\partial t} = -\frac{c}{n}\frac{\partial \hat{v}^g}{\partial x_1}$ in Eqs. (9) and (10) and assume that the right-hand side $\frac{1}{n}u|_{y=H}$ and $\frac{1}{n}v|_{y=H}$ of the no-slip conditions (8) is a negligible value. We solve Eqs. (8)–(12) independently from the governing equations of the liquid film flow (see Appendix A for details). This is a linear system where the Fourier harmonic H^k of the film thickness $H(x_1)$ generates the corresponding gas reaction $(F^k(y),\ P_g^k(y))$. Taking into account Eq. (11), the perturbation fields $\hat{u}^g$, $\hat{v}^g$, $\hat{P}^g$ are as follows:

$$\hat{u}^g(x_1,y) = -\sum_{k=-N/2+1}^{N/2-1} \frac{dF^k}{dy} H^k \exp(2\pi i k x_1), \quad \left(F^{-k}\right)^* = F^k; \tag{13}$$

$$\hat{v}^g(x_1,y) = \sum_{k=-N/2+1}^{N/2-1} 2\pi i k F^k(y) H^k \exp(2\pi i k x_1); \tag{14}$$

$$\hat{P}^g(x_1,y) = \sum_{k=-N/2+1}^{N/2-1} P_g^k(y) H^k \exp(2\pi i k x_1), \quad \left(P_g^{-k}\right)^* = P_g^k. \tag{15}$$

Thus, we reduce the two-phase problem to the solving of the liquid film flow Eqs. (1)–(5) with the modified boundary conditions (6) and (7) (see Appendix A) where we take into account the turbulent gas reaction to the wavy interface. The free surface shape is unknown beforehand and the coordinates transformation $x_1 = x - ct$, $\eta = y/H$ allows us to define the flow area: $x_1 \in [0,1]$, $\eta \in [0,1]$. We use spectral method to obtain the steady-state solutions of Eqs. (1)–(7) and Appendix A gives the numerical algorithm details.

There are eight parameters in Eqs. (1)–(12) – ε, ε_2, ε_μ, ε_ρ, n, Fi, Re, Re^g. It is easy to see that $n = \frac{\varepsilon_2 \varepsilon_\mu}{\varepsilon_\rho}\frac{\mathrm{Re}^g}{\mathrm{Re}}$ and only seven parameters are independent. We will use λ_{neut}/L, Ka, Re, $\sqrt{\sigma/\rho g(1-\varepsilon_\rho)}/D$, ε_μ, ε_ρ, Re^g as the independent parameters for the calculations below, where λ_{neut} is the wavelength of the neutral disturbance of the wavyless solution and $\mathrm{Ka} \equiv Fi^{1/11}$, Ka is the Kapitsa number. It is evident that $\lambda_{neut} = H_0 f(\mathrm{Ka}, \mathrm{Re}, \sqrt{\sigma/\rho g(1-\varepsilon_\rho)}/D, \varepsilon_\mu, \varepsilon_\rho, \mathrm{Re}^g)$ and the equations parameters may be defined using our independent parameters – $\varepsilon = (H_0/\lambda_{neut})(\lambda_{neut}/L)$, $\varepsilon_2 = (3\mathrm{Re}/\mathrm{Ka})^{1/3}(\sqrt{\sigma/\rho g(1-\varepsilon_\rho)}/D)/\mathrm{Ka}^{3/2}$.

Our choice of the independent parameters set has several advantages. Values of the parameters Ka, $\sqrt{\sigma/\rho g(1-\varepsilon_\rho)}/D$, ε_μ, ε_ρ depend only on the liquid/gas physical properties and on the gas channel geometry. Only values of the parameters Re and Re^g vary with the liquid/gas flow rate changing. Choice of the value λ_{neut}/L as the independent parameter allows us to compare the results of the Navier–Stokes calculations with the predictions of different integral and asymptotic approaches where the value of the neutral wavelength is different.

Let us draw attention that the averaged liquid flow rate is held constant in our calculations. Taking into account the kinematic condition (5) and the no-slip conditions (4) the integration of the continuity Eqs. (3) gives

$$q(x_1) - cH(x_1) = const = < q > - c < H > = 1 - c < H >,$$
$$q(x_1) \equiv H(x_1) \int_0^1 u d\eta.$$

Here $<\cdots>$ is the value averaged over a wavelength. We use this equation in our computations of the steady-state solutions (see Appendix A). The constant-flux formulation corresponds to the experimental situation. This formulation is much closer to the reality where the mass conservation takes place during a spatial–temporal evolution.

3. Results of the calculations

Fig. 2 demonstrates the main characteristics of the nonlinear steady-state solutions that branched from the basic solution at three values of the superficial gas velocity. We present also the wavy profiles of the solution film thickness and the contour lines of the streamline function $\Psi(x,\eta) = \int_0^\eta (c-u) H d\eta'$ in a moving coordinate system. The liquid particle trajectory coincides with the contour lines in a coordinate system moving with the solution

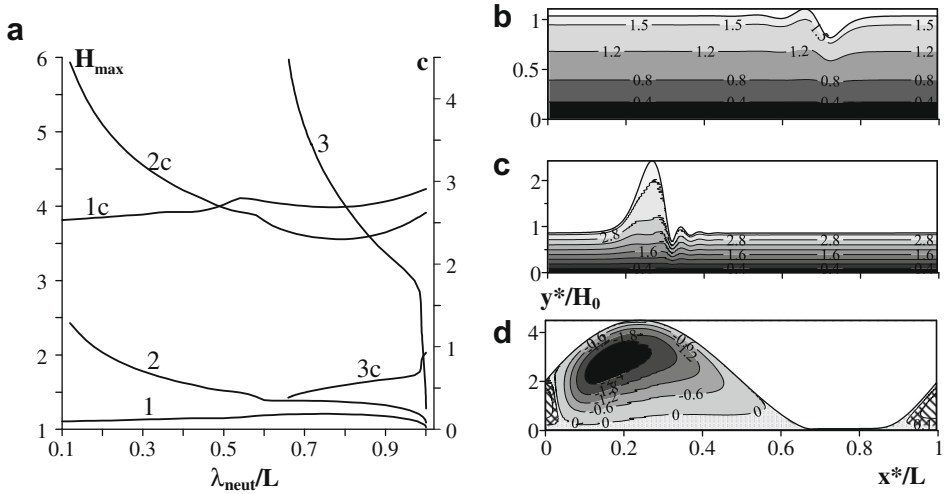

Fig. 2. Maximal value of wavy film thickness (lines 1–3), and phase velocity (lines 1c–3c) of nonlinear wavy regimes branched from the trivial solution as a function of wavelength. Contour lines of the streamline function (figures b–d) in a reference frame that moves with the wave phase velocity. Here Re = 5, air/water system; Lines 1, 1c correspond to U_{GS} = 3 m/s; 2, 2c – U_{GS} = 6 m/s; 3, 3c – U_{GS} = 10.6 m/s. Figure (b) corresponds to $\lambda_{neut}/L = 0.12$ and U_{GS} = 3 m/s; (c) $\lambda_{neut}/L = 0.12$ and U_{GS} = 6 m/s; and (d) $\lambda_{neut}/L = 0.75$ and U_{GS} = 10.6 m/s.

phase velocity. The computations correspond to air/water system Ka = 9.2615, ε_μ = 0.0182, ε_ρ = 0.0012, $\sqrt{\sigma/\rho g}/D = 0.2765$ at Re = 5. At small value of U_{GS} = 3 m/s, the nonlinear solutions are close to the waves on the surface of a liquid film freely falling down under an action of gravity (see paper by Trifonov (2008)). In this case, the "long wave" looks like a succession of "solitary dips" (see Fig. 2b). At moderate value of U_{GS} = 6 m/s, we found that the "long wave" of the family branched from the trivial solution looks like a succession of "solitary humps" (see Fig. 2c) and the interfacial shear changes qualitatively the solution type. At large value of U_{GS} = 10.6 m/s, the family branched from the basic solution has no continuation into the region of "long" waves. The waves demonstrate a rapid increasing of the maximal film thickness starting from a finite value of the wavelength (see line 3 in Fig. 2) and the contour lines of the streamline function demonstrate an internal vortex (see Fig. 2d).

Thus, there are the values of the superficial gas velocity where we have no steady-state traveling solutions with small values of λ_{neut}/L. Minimal value of these velocities will correspond to the onset of flooding. We start with the "long wave" ($\lambda_{neut}/L = 0.15$) at moderate value of the superficial gas velocity and, using a continuation method, we increase (or decrease) values of U_{GS} to obtain dependences in Fig. 3. We carry out these computations for two values of the liquid Reynolds number (Fig. 3a and b) and for three different systems – air/water, helium/water (ε_μ = 0.02, ε_ρ = 0.0001653) and hydrogen/water (ε_μ = 0.00886, ε_ρ = 0.0000833). In Figs. 4–6, we present the wavy profiles of the solution film thickness and the contour lines of the $u(x, \eta)$ component velocity (in a laboratory coordinate system). With the superficial gas velocity increasing, the wave amplitude increases as it shown in Figs. 3–6. At the same time, the wave velocity decreases with increasing in U_{GS}. The u-velocity distribution in Figs. 4–6 demonstrates a region of flow reversal near the film thickness minimum at small and moderate values of U_{GS}. At large value of U_{GS}, the negative u-velocities exist near the film thickness maximum and we can see the "large" waves moving over a thin sublayer. Amplitude of the "large" waves is several times bigger than the wave amplitude at small value of superficial gas velocity (see Figs. 4–6). We found that the negative u-velocity around the film thickness maximum appears at small neighbourhood of the "returning point" (U^f_{GS}) of the dependences in Fig. 3 where the derivatives dH_{max}/dU_{GS} and dc/dU_{GS} change sign. We did not obtain solutions at $U_{GS} > U^f_{GS}$

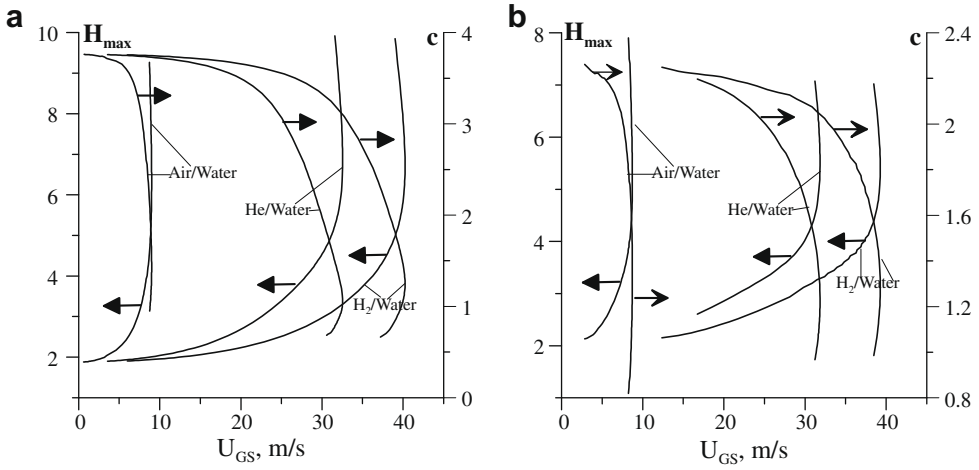

Fig. 3. Maximal value of wavy film thickness and phase velocity of nonlinear wavy regimes as a function of gas superficial velocity at $\lambda_{neut}/L = 0.15$ for different gases (figure (a) corresponds to Re = 10 and (b) Re = 40).

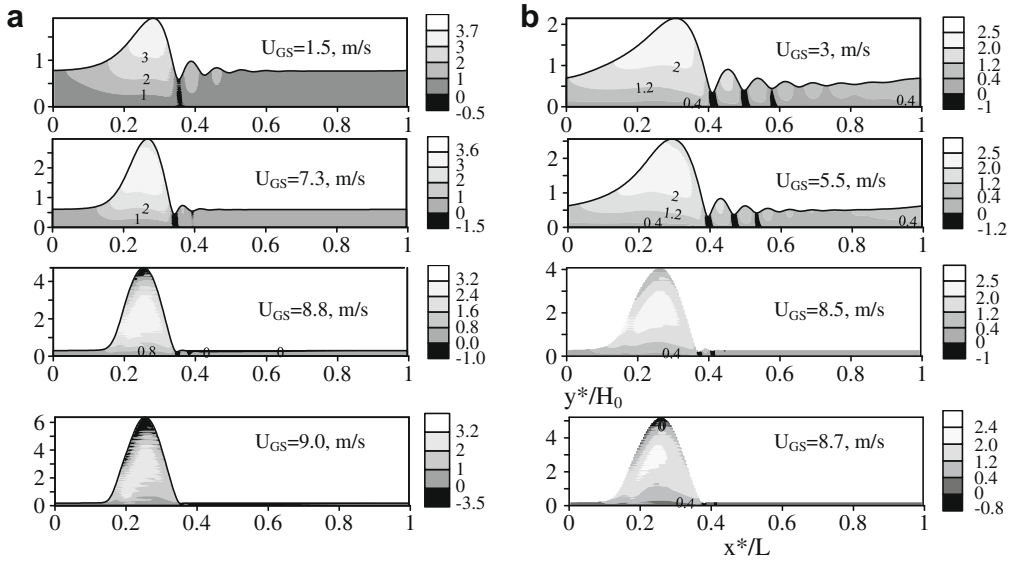

Fig. 4. Contour lines of the liquid u-velocity in the case of air–water at different values of superficial gas velocity. Here $\lambda_{neut}/L = 0.15$ and figures (a) correspond to Re = 10 and (b) 40.

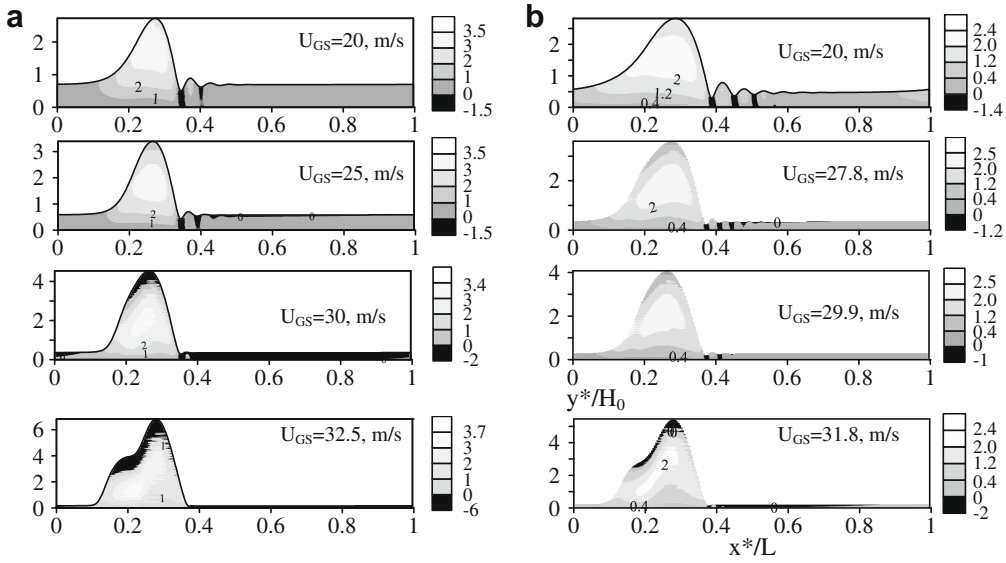

Fig. 5. Contour lines of the liquid u-velocity in the case of helium-water at different values of superficial gas velocity. Here $\lambda_{neut}/L = 0.15$ and figures (a) correspond to Re = 10 and (b) 40.

and this is why we call the point (U^f_{GS}) as the "returning point". There are two solutions in a small neighbourhood of the "returning point" at one value of the superficial velocity. We obtain the "returning points" for all values of the liquid Reynolds number considered in the paper and for all values of the distance between the plates and the gas/liquid physical parameters. Further, we consider the "returning point" as a definition of the onset of flooding.

In accordance with the nondimensional parameters of our equations, the flooding curve is a function of five variables and has the form as follows:

$$\mathrm{Re}^{gf} = \mathrm{Re}^{gf}(\mathrm{Re}, \mathrm{Ka}, \sqrt{\sigma/\rho g(1-\varepsilon_\rho)}/D, \varepsilon_\mu, \varepsilon_\rho).$$

We compute the flooding curves over a wide range of the independent parameters using a continuation method. We present these results in Figs. 7 and 8a by solid lines. To obtain these curves we start with the flooding point for the air/water system and varying one of the nondimensional parameters we compute the returning point U^f_{GS}. Value of the gas superficial velocity is an additional unknown and we solve an equation $dc/dU_{GS} = 0$ simultaneously with Eqs. (A1)–(A12) to find the flooding curves. The systematic computation of the flooding curves allows us to suggest correlation:

$$\mathrm{Re}^{gf} = \frac{U^f_{GS} D_e}{4\nu_g} = \frac{2.35\varepsilon_\rho^{0.37}\mathrm{Ka}^{2.37}}{\varepsilon_\mu^{0.73}\mathrm{Re}^{0.03}(\sqrt{\sigma/\rho g(1-\varepsilon_\rho)}/D)^{1.15}}. \quad (16)$$

We use a special numerical algorithm to obtain the values of the coefficient and five powers in this equation. To find six unknowns we minimize the deviation between the curves in Figs. 7 and 8a and the predictions of equation where the coefficient and five powers are variables. We use all array of individual points $(\mathrm{Re}^{gf}_{calc})_i$ of the onset of flooding calculated using fundamental Eqs. (A1)–(A12). Total amount of the points to plot curves in Figs. 7 and 8a is around seven hundreds ($i = 1, 2, \ldots, 700$). Thus, we look for the minimum

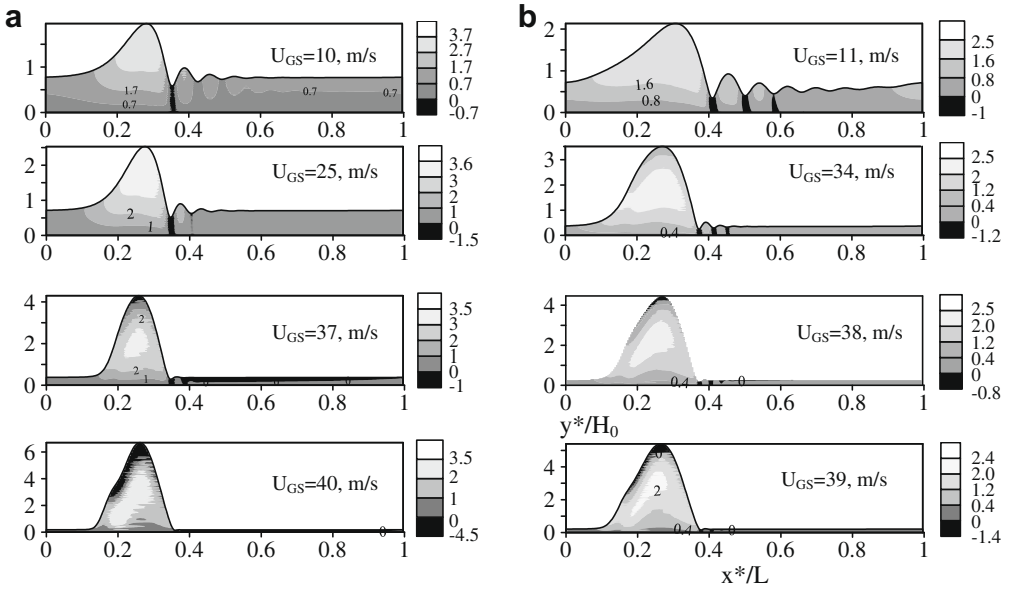

Fig. 6. Contour lines of the liquid u-velocity in the case of hydrogen-water at different values of superficial gas velocity. Here $\lambda_{neut}/L = 0.15$ and figures (a) correspond to Re = 10 and (b) 40.

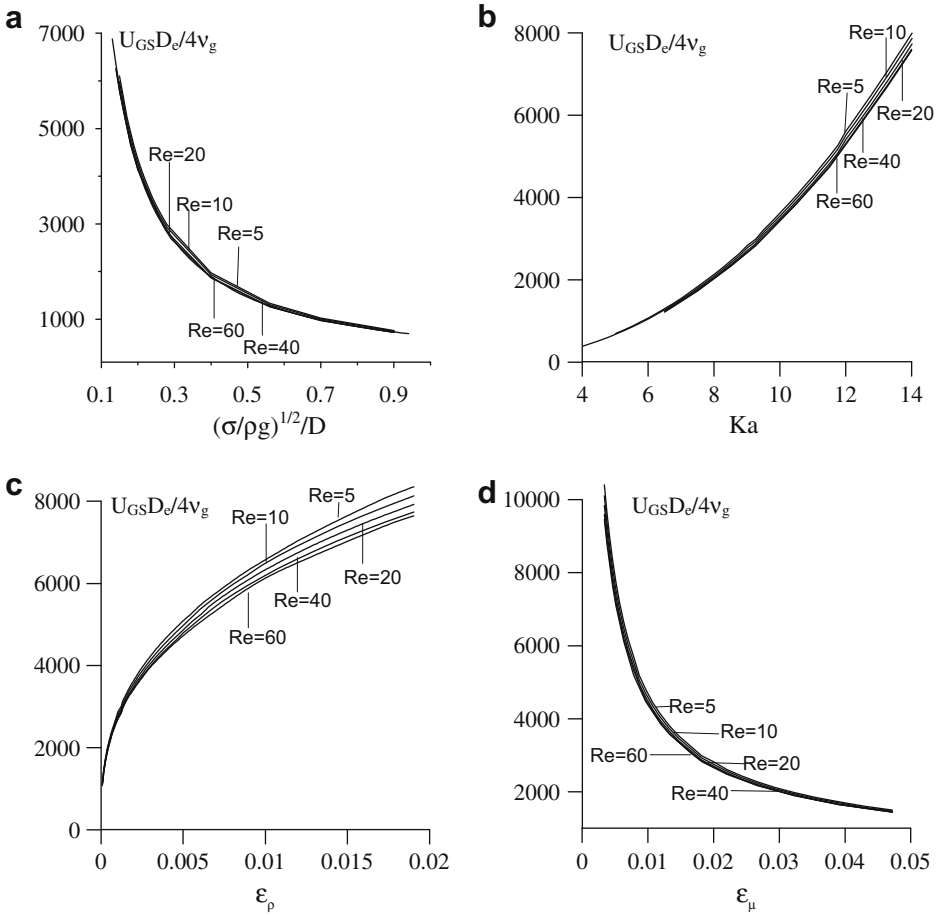

Fig. 7. Gas superficial velocities of the onset of flooding versus the dimensionless parameter at different values of the liquid Reynolds number. Here (a) corresponds to $\varepsilon_\rho = 0.0012$, Ka = 9.2615, $\varepsilon_\mu = 0.0182$; (b) $\varepsilon_\rho = 0.0012$, $(\sigma/\rho g)^{1/2}/D = 0.2765$, $\varepsilon_\mu = 0.0182$; (c) Ka = 9.2615, $(\sigma/\rho g)^{1/2}/D = 0.2765$, $\varepsilon_\mu = 0.0182$; and (d) $\varepsilon_\rho = 0.0012$, Ka = 9.2615, $(\sigma/\rho g)^{1/2}/D = 0.2765$.

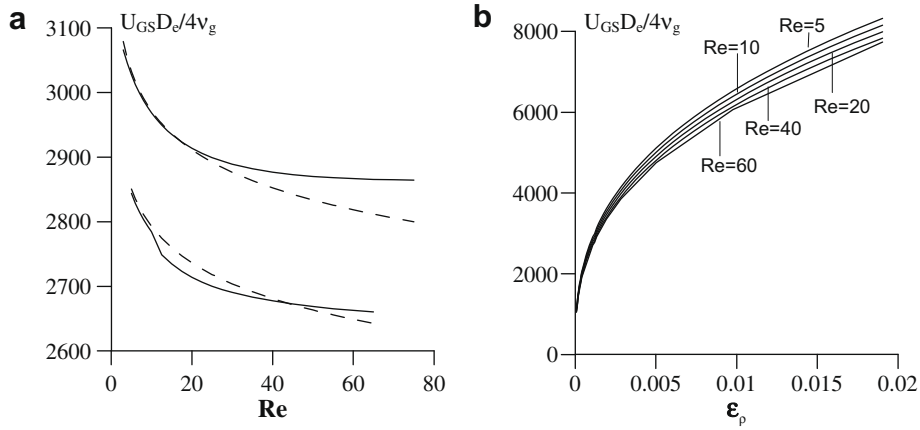

Fig. 8. Gas superficial velocities of the onset of flooding versus the dimensionless parameter. Lines 1 in figure (a) corresponds to $(\sigma/\rho g)^{1/2}/D = 0.2765$, $\varepsilon_\mu = 0.0182$, $\varepsilon_\rho = 0.0012$ and Ka = 9.2615; lines 2 $(\sigma/\rho g)^{1/2}/D = 0.204$, $\varepsilon_\mu = 0.0167$, $\varepsilon_\rho = 0.00123$ and Ka = 7.5534. Dashed lines in figure (a) corresponds to Eq. (16). Figure (b) corresponds to Eq. (16) at the same values of parameters as in Fig. 7c.

of function of six variables that can be expressed as a sum of squared functions:

$$\Psi(b, b_1, \ldots, b_5) = \sum_{i=1}^{700} \left(\mathrm{Re}^{gf}_{pred} - \mathrm{Re}^{gf}_{calc}\right)^2_i;$$

$$\mathrm{Re}^{gf}_{pred} = b\varepsilon_\rho^{b_1}\mathrm{Ka}^{b_2}\varepsilon_\mu^{b_3}\mathrm{Re}^{b_4}\left(\sqrt{\sigma/\rho g(1-\varepsilon_\rho)}/D\right)^{b_5}.$$

We calculate $(\mathrm{Re}^{gf}_{pred})_i$ at the same values of $[\varepsilon_\rho, \mathrm{Ka}, \varepsilon_\mu, \mathrm{Re}, (\sqrt{\sigma/\rho g(1-\varepsilon_\rho)}/D)]$ as the corresponding values of the parameters of point i in Figs. 7 and 8a.

Comparisons between the Figs. 8b and 7c and between the dashed and solid lines in Fig. 8a demonstrate validity of the obtained six coefficients. Let us emphasize that we do not use any experimental data to define coefficients in Eq. (16). We extract them from the computations based on the fundamental equations and principles.

There are many correlations in literature where the authors present the empirical flooding dependences in terms of dimensionless velocities $U^*_G \equiv U^f_{GS}\sqrt{\varepsilon_\rho}/\sqrt{gD(1-\varepsilon_\rho)}$, $U^*_L \equiv U^f_{LS}/\sqrt{gD(1-\varepsilon_\rho)}$. Drosos et al. (2006) describe their water data on the onset of flooding using the Wallis-type expression:

$$\sqrt{U^*_G} + 0.708\sqrt{U^*_L} = 1.136.$$

Zapke and Kröger (2000b) based on the results of experiments with different fluids propose another type of the correlation for a vertical rectangular duct:

$$U^*_G = 0.0742\frac{1}{Oh^{0.15}}\left(\frac{1}{U^*_L}\right)^{0.2}.$$

The Ohnesorge number, used in their paper, is $Oh \equiv \sqrt{\mu^2/(\rho D\sigma)} = \mathrm{Ka}^{-11/4}We^{1/4}$ and the Weber number is $We = \sigma/(\rho g(1-\varepsilon_\rho)D^2)$. Range of the liquid flow rates in both experiments of Drosos et al. (2006) and Zapke and Kröger (2000a,b) was $10^{-3} \leqslant U^*_L \leqslant 0.062$.

There are many correlations in literature where the Kutateladze number $Ku_G \equiv U^f_{GS}\sqrt{\rho_g}/(g\sigma(\rho-\rho_g))^{1/4}$ is used to describe the onset of flooding (see the review by McQuillan and Whalley (1985)). Pushkina and Sorokin (1969) carried out experiments with water, glycerine and ethyl alcohol using tubes of different diameters. Range of the liquid flow rates in their experiments was $10^{-5} \leqslant U^*_L \leqslant 0.1$. To describe flooding data they suggested correlation as follows:

$$Ku_G = U^*_G We^{-1/4} = 3.2.$$

Wallis and Kuo (1976) obtained the correlation $Ku_G = 1.87$ for the onset of flooding using the Bernouilli equations. In accordance with McQuillan and Whalley (1985) conclusions, the most successful empirical correlation was that of Alekseev et al. (1972), which works well over a range of tube diameters, liquid flow rates $(U^*_L \leqslant 1)$ and liquid surface tensions:

$$Ku_G = U^*_G We^{-1/4} = \frac{0.3}{(1-\varepsilon_\rho)^{0.11}}\left(\frac{1}{U^*_L}\right)^{0.22}We^{-0.095}.$$

In accordance with McQuillan and Whalley (1985), the most successful theoretical correlation is a modified form of the correlation presented by Bharathan et al. (1978):

$$\frac{2f_w(U^*_L)^2}{(1-\alpha)^2} + \frac{2fi(U^*_G)^2}{\alpha^{2.5}} = 1-\alpha, \quad f_w = 0.005,$$

$$fi = f_w + 14.6(1-\alpha)^{1.87}.$$

Here α is a void fraction that can be expressed as $\alpha = 1 - 4.58^*(U^*_L)^{1/3}We^{1/4}\mathrm{Ka}^{-11/12}$.

In terms of U^*_G, U^*_L, Eq. (16) is

$$Ku_G = U^*_G We^{-1/4} = \frac{4.793\varepsilon_\mu^{0.27}}{\varepsilon_\rho^{0.135}\mathrm{Ka}^{0.463}}\left(\frac{1}{U^*_L}\right)^{0.03}We^{-0.0525}. \quad (17)$$

Fig. 9 shows comparison between the correlations for the air/water system at $D = 10$ mm. The detailed comparison of Eqs. (16) and (17) predictions with the experimental data for different liquids and diameters is a goal of separate investigation. Here we only note that

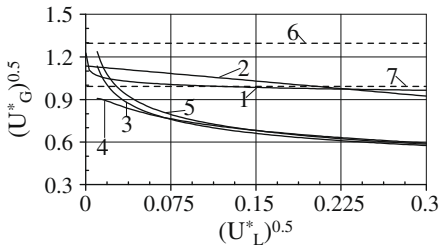

Fig. 9. Comparison of the proposed equation for the onset of flooding with both empirical and theoretical flooding correlations for the air/water system. Line 1 corresponds to Eq. (16) or (17); 2 – Drosos et al. (2006); 3 – Zapke and Kröger (2000b); 4 – Bharathan et al. (1978); 5 – Alekseev et al. (1972); 6 – Pushkina and Sorokin (1969); and 7 – Wallis and Kuo (1976).

with the distance between the plates increasing, the nondimensional flooding velocity U_G^* decreases in accordance with Eq. (17) and that agrees with the experimental results of Sudo et al. (1991) and Vlachos et al. (2001).

There is a limitation of the simplified Benjamin-Miles approach used in the paper regarding the small liquid-to-gas velocity ratio, $n \gg 1$. This limitation can be written as follows:

$$n = \frac{\varepsilon_2 \varepsilon_\mu}{\varepsilon_\rho}\frac{\mathrm{Re}^{gf}}{\mathrm{Re}} \gg 1, \quad \frac{\mathrm{Re}^{gf}}{\mathrm{Re}} = \frac{\sqrt{\varepsilon_\rho}}{\varepsilon_\mu}\frac{U_G^*}{U_L^*}, \quad \varepsilon_2 = \left(\frac{3\mathrm{Re}}{\mathrm{Ka}}\right)^{1/3}\frac{\sqrt{We}}{\mathrm{Ka}^{3/2}},$$
$$n = \left(\frac{3}{2}\right)^{1/3}\frac{1}{\mathrm{Ka}^{11/12}}\left(\frac{1}{U_L^*}\right)^{2/3}\frac{\sqrt{We}}{\sqrt{\varepsilon_\rho}}Ku_G. \tag{18}$$

In the case of air/water system and for $D = 10$ mm, Eqs. (17) and (18) gives $n = 1.95$ at $U_L^* = 1$, $n = 3.16$ at $U_L^* = 0.5$, $n = 9.7$ at $U_L^* = 0.1$ and $n = 48.2$ at $U_L^* = 0.01$. We may conclude that the assumption $n \gg 1$ is valid up to the values of $U_L^* \approx 0.1$ for the air/water system and $D = 10$ mm. The assumption is valid at higher values of U_L^* with the distance between the plates decreasing.

4. Conclusions

We considered the counter-current wavy gas/liquid film flow between vertical plates. We used the Navier–Stokes equations in their full statement to describe the liquid phase hydrodynamics. For the gas phase equations, we used the simplified Benjamin-Miles approach where the liquid phase is a small disturbance for the turbulent gas flow. Our goal was to predict theoretically flooding onset using the fundamental equations and principles. We varied the liquid Reynolds number, wavelength and the gas superficial velocity to see what happening with the steady-state traveling solutions when the parameters were close to the experimental flooding condition.

We obtained that there were six independent parameters to describe the gas/liquid wavy dynamics – Ka, Re, Re^g, $\sqrt{\sigma/\rho g(1-\varepsilon_\rho)}/D$, ε_μ, ε_ρ, $\mathrm{Ka} = ((\sigma/\rho)^3/g(1-\varepsilon_\rho)\nu^4)^{1/11}$ is the Kapitza's number, D is a distance between the plates, $\varepsilon_\mu = \mu_g/\mu$ and $\varepsilon_\rho = \rho_g/\rho$.

We found that with the superficial gas velocity increasing and starting from some value of the velocity, the waves demonstrate a rapid decrease of both the minimum film thickness and the phase wave velocity. At the same time, the maximum film thickness increases and finally the wave structure demonstrates the negative u-velocities in the neighbourhood of the maximum. At smaller values of the superficial velocity, the negative u-velocities take place in the neighbourhood of the film thickness minimum. Both the wave celerity and the film thickness minimum are still positive numbers at such values of the superficial gas velocity. The described transformation of the wave structure with the superficial gas velocity increasing takes place for different gas/liquid systems considered in the paper (air/water, argon/water and hydrogen/water). We found a region of the "returning point" of the superficial velocity where we have several solutions and where the flooding takes place. We did not obtain the steady-state traveling solutions when the superficial gas velocity is greater than the value corresponding to the "returning point". These findings allowed us to define the onset of flooding mathematically and to obtain its dependence on the two-phase flow parameters. We obtained new flooding correlation that based on the fundamental equations and principles of the gas/liquid interaction.

Appendix A

We consider the steady-state traveling solutions of Eqs. (1)–(12). The coordinates transformation $x_1 = x - ct$, $\eta = y/H(x-ct)$ defines the flow area: $x_1 \in [0, 1]$, $\eta \in [0, 1]$ and allows us to write the governing equations as follows (further, we omit the subscript '1'):

$$c\frac{\partial u}{\partial x} + \eta_x c\frac{\partial u}{\partial \eta} - \frac{\partial P}{\partial x} - \eta_x\frac{\partial P}{\partial \eta} + \frac{1}{\varepsilon \mathrm{Re}}\left[3 - \lambda^f \varepsilon_2 \varepsilon_\rho n^2 \mathrm{Re} + \eta_y^2\frac{\partial^2 u}{\partial \eta^2} + \varepsilon^2\left(\frac{\partial^2 u}{\partial x^2} + \eta_x^2\frac{\partial^2 u}{\partial \eta^2} + 2\eta_x\frac{\partial^2 u}{\partial x \partial \eta} + (\eta_{x\xi} + \eta_x\eta_{x\eta})\frac{\partial u}{\partial \eta}\right)\right] - \eta_y\frac{\partial u v}{\partial \eta} - \frac{\partial u^2}{\partial x} - \eta_x\frac{\partial u^2}{\partial \eta} = 0; \tag{A1}$$

$$-\eta_y\frac{\partial P}{\partial \eta} + \frac{\varepsilon}{\mathrm{Re}}\left[\eta_y^2\frac{\partial^2 v}{\partial \eta^2} + \varepsilon^2\left(\frac{\partial^2 v}{\partial x^2} + \eta_x^2\frac{\partial^2 v}{\partial \eta^2} + 2\eta_x\frac{\partial^2 v}{\partial x \partial \eta} + (\eta_{x\xi} + \eta_x\eta_{x\eta})\frac{\partial v}{\partial \eta}\right)\right] - \varepsilon^2\left(-c\frac{\partial v}{\partial x} - \eta_x c\frac{\partial v}{\partial \eta} + \frac{\partial u v}{\partial x} + \eta_x\frac{\partial u v}{\partial \eta} + \eta_y\frac{\partial v^2}{\partial \eta}\right) = 0; \tag{A2}$$

$$v(x,\eta) = -H(x)u(x,\eta)\eta_x - \frac{\partial}{\partial x}\left(H\int_0^\eta u(x,\eta')d\eta'\right); \tag{A3}$$

$$H(x)\int_0^1 (u(x,\eta') - c)d\eta' = 1 - c\langle H\rangle; \tag{A4}$$

$$u(x,\eta) = 0, \quad \eta = 0; \tag{A5}$$

$$P - \varepsilon_\rho n^2 \hat{P}^g\Big|_{y=0} = \frac{2\varepsilon}{\mathrm{Re}}\left(\eta_y\frac{\partial v}{\partial \eta} - \varepsilon_\mu n\frac{\partial \hat{v}^g}{\partial y}\Big|_{y=0}\right)\frac{1 + \varepsilon^2\left(\frac{dH}{dx}\right)^2}{1 - \varepsilon^2\left(\frac{dH}{dx}\right)^2} - \varepsilon^2\frac{(3Fi)^{1/3}}{\mathrm{Re}^{5/3}}\frac{\frac{d^2H}{dx^2}}{\left[1 + \varepsilon^2\left(\frac{dH}{dx}\right)^2\right]^{3/2}}, \quad \eta = 1; \tag{A6}$$

$$\eta_y\frac{\partial u}{\partial \eta} + \varepsilon^2\left(\frac{\partial v}{\partial x} + \eta_x\frac{\partial v}{\partial \eta}\right) + 4\varepsilon^2\eta_y\frac{\partial v}{\partial \eta}\frac{\frac{dH}{dx}}{1 - \varepsilon^2\left(\frac{dH}{dx}\right)^2} = -\frac{\lambda^f}{2}\varepsilon_\rho n^2 \mathrm{Re} + \varepsilon_\mu n\left[\frac{\partial \hat{u}^g}{\partial y}\Big|_{y=0} + \frac{d^2 u_b^g}{dy^2}\Big|_{y=0}H + 4\varepsilon^2\frac{\partial \hat{v}^g}{\partial y}\Big|_{y=0}\frac{\frac{dH}{dx}}{1 - \varepsilon^2\left(\frac{dH}{dx}\right)^2}\right], \quad \eta = 1. \tag{A7}$$

Here $\langle\cdots\rangle$ is the value averaged over a wavelength, $\eta_y = 1/H$, $\eta_x = -\eta(dH/dx)/H$, $\eta_{x\eta} = -\eta_y dH/dx$, $\eta_{x\xi} = -\eta_y(\eta_x dH/dx + \eta d^2H/dx^2)$, λ^f is the smooth channel friction coefficient for the gas turbulent flow and the dimensionless value of the basic pressure is $P_b^g = \frac{\lambda^f \varepsilon_2 x}{\varepsilon}$. We take into account that the basic velocity profile agrees with the friction coefficient definition – $\frac{du_b^g}{dy}\Big|_{y=0} = -0.5\lambda^f \varepsilon_2 \mathrm{Re}^g$ and $n\varepsilon_\rho \mathrm{Re} = \varepsilon_2\varepsilon_\mu \mathrm{Re}^g$.

Functions H, u, v, P are periodic over the coordinate x and they are unknowns. We use spectral method to obtain the steady-state solutions of Eqs. (A1)–(A7):

$$u(x,\eta) = \frac{1}{2}U_1(x) + \sum_{m=2}^{M} U_m(x)T_{m-1}(\eta_1), \eta_1 = 2\eta - 1,$$
$$U_m(x) = U_m^0 + \sum_{\substack{k=-N/2+1 \\ k\neq 0}}^{N/2-1} U_m^k \exp(2\pi i k x), (U_m^{-k})^* = U_m^k, \quad m = 1,\ldots,M.$$

$$H(x) = H^0 + \sum_{\substack{k=-N/2+1 \\ k\neq 0}}^{N/2-1} H^k \exp(2\pi i k x), \quad (H^{-k})^* = H^k.$$

Here $T_m(\eta_1)$ are Chebyshev polynomials and the 'star' superscript designates complex conjugation.

The numerical algorithm starts with the specification of the initial approximation for harmonics U_m^k, H^k and for the value of $\boldsymbol{c}$. There is a symmetry in the equations with respect to the coordinate shift $x \to x + const$. The phase of one of the film thickness

harmonics can be defined beforehand due to this symmetry (for example $Real(H^1)$=0). The value of the phase velocity $\boldsymbol{c}$ will be unknown instead of $Real(H^1)$.

At $(M+1)(N-1)$ known values of U_m^k, c, H^k, the velocity $v(x,\eta)$ is unambiguously regenerated from Eq. (A3), $P(x,\eta)$ – from Eqs. (A2) and (A6). Using the Newton's iterative method and Eqs. (A1) and (A4) transformed into $(k,\ m)$-space, we improve the initial approximation of the unknowns $\left(U_m^k,\ H^k,\ c\right)$. We use the first order differential scheme to calculate the Jacoby matrix. Taking into account the boundary conditions (A5) and (A7), we have $(M+3)(N-1)$ nonlinear algebraic equations to obtain $(M+1)(N-1)$ unknown values. The basis functions in the spectral expansion do not satisfy the boundary conditions and that is why the number of unknowns is less than the number of equations. We discard $2(N-1)$ equations corresponding to the last two Chebyshev coefficients in the expansion of Eq. (A1). The results will be correct at a good enough accuracy of approximation of the functions $u(x,\eta)$ – $|U_m^{N/2-1}|/\sup|U_m^k| < 10^{-3}$ at any m, and $|U_M^k|/\sup|U_m^k| < 10^{-3}$ at any k. During the calculations, the corresponding increasing N and M (we varied value of N from 8 to 256 and value of M – from 5 to 50, depending on the parameters) maintained the indicated conditions.

To calculate the gas reaction on the wavy liquid film we substitute Eqs. (13)–(15) into the governing Eqs. (8)–(12):

$$2\pi ik\varepsilon\varepsilon_2\mathrm{Re}^g\left[\frac{d^2u_b^g}{dy^2}F^k+u_b^g\varepsilon^2(2\pi k)^2F^k-u_b^g\frac{d^2F^k}{dy^2}\right]=-\frac{d^4F^k}{dy^4}+2\varepsilon^2(2\pi k)^2\frac{d^2F^k}{dy^2}-\varepsilon^4(2\pi k)^4F^k; \tag{A8}$$

$$\left.\frac{dF^k}{dy}\right|_{y=0}=\left.\frac{du_b^g}{dy}\right|_{y=0};\quad F^k\Big|_{y=0}=0;\quad \left.\frac{d^2F^k}{dy^2}\right|_{y=0.5/\varepsilon_2}=F^k\Big|_{y=0.5/\varepsilon_2}=0; \tag{A9}$$

$$P_g^k=u_b^g\frac{dF^k}{dy}-\frac{du_b^g}{dy}F^k-\frac{i}{2\pi k\varepsilon\varepsilon_2\mathrm{Re}^g}\left[-\frac{d^3F^k}{dy^3}+(2\pi k\varepsilon)^2\frac{dF^k}{dy}\right]; \tag{A10}$$

$$u_b^g=\begin{cases}-\eta\sqrt{\lambda^f/2}, \eta<8.74^{7/6}\\ -8.74\eta^{1/7}\sqrt{\lambda^f/2}, \eta>8.74^{7/6}\end{cases},\quad \lambda^f=\frac{0.3164}{(4\mathrm{Re}^g)^{1/4}};$$
$$\eta\equiv\varepsilon_2 y\mathrm{Re}^g\sqrt{\lambda^f/2}. \tag{A11}$$

To find functions $F^k(y)$ we solve these equations numerically for $k=1,2,\ldots,N/2-1$. Method uses the Chebyshev-series to solve a two-point boundary problem (A8) and (A9).

Eq. (A11) are the well-known velocity distribution for the turbulent flow $(u_b^g)^*/v_*=8.74(y^*v_*/v_g)^{1/7},\ v_*=\sqrt{\tau_g/\rho_g}, \eta\equiv y^*v_*/v_g$ and the Blasius formula for the friction coefficient. Here λ^f is the friction coefficient and we take into account that the hydraulic diameter of our duct is $2D$. The dimensional pressure and the interfacial shear are as follows:

$$(P_b^g)^*\equiv\frac{\lambda^f}{2D}\frac{\rho_gU_{GS}^2}{2}x^*=\frac{2\tau_g}{D}x^*,\quad \tau_g\equiv\mu_g\left.\frac{d(u_b^g)^*}{dy^*}\right|_{y^*=0}=\lambda^f\frac{\rho_gU_{GS}^2}{8}. \tag{A12}$$

Dimensionless value of the basic pressure is $P_b^g=\frac{\lambda^f\varepsilon_2x}{\varepsilon}$. Velocity profile (A11) agrees with the condition (A12) – $\left.\frac{du_b^g}{dy}\right|_{y=0}=-0.5\lambda^f\varepsilon_2\mathrm{Re}^g$.

Eqs. (13), (14), (A9) and (A10) give

$$\left.\frac{\partial\hat{v}^g}{\partial y}\right|_{y=0}=\frac{dH}{dx}\left.\frac{du_b^g}{dy}\right|_{y=0};$$

$$\hat{P}^g\Big|_{y=0}=-\sum_{k=-N/2+1}^{N/2-1}\frac{i}{2\pi k\varepsilon\varepsilon_2\mathrm{Re}^g}\left[-\left.\frac{d^3F^k}{dy^3}\right|_{y=0}+(2\pi k\varepsilon)^2\left.\frac{du_b^g}{dy}\right|_{y=0}\right]H^k\exp(2\pi ikx).$$

We use these equations in our modified boundary conditions (A6) and (A7) to take into account the gas reaction on the liquid film hydrodynamics.

References

Alekseenko, S.V., Nakoryakov, V.E., Pokusaev, B.G., 1985. Wave formation on a vertical falling liquid film. AIChE J. 31, 1446–1460.

Alekseev, V.P., Poberezkin, A.E., Gerasimov, P.V., 1972. Determination of flooding rates in regular packing. Heat Transfer Soviet Res. 4, 159–163.

Benjamin, T.B., 1959. Shearing flow over a wavy boundary. J. Fluid Mech. 6, 161–205.

Bharathan, D., Wallis, G.B., Richter, H.J., 1978. Air–water countercurrent annular flow in vertical tubes. EPRI Report No. EPRI NP-786.

Biage, M., Delhaye, J.M., Vernier, P., 1989. The flooding transition: a detailed experimental investigation of the liquid film before the flooding point. In: ANS Proceedings, National Heat Transfer Conference, ANS, pp. 53–60.

Chu, K.I., Dukler, A.E., 1974. Statistical characteristics of thin wavy films. AIChE J. 20, 695–706.

Demekhin, E.A., Tokarev, G.Y., Shkadov, V.Y., 1989. Instability and nonlinear waves for the vertical counter-current flow of a liquid film and turbulent gas. TOKhT 23, 64–70.

Drosos, E.I.P., Paras, S.V., Karabelas, A.J., 2006. Counter-current gas–liquid flow in a vertical narrow channel – liquid film characteristics and flooding phenomena. Int. J. Multiphase Flow 32, 51–81.

Dukler, A.E, Smith, L., 1977. Two phase interactions in countercurrent two phase flow: studies of the flooding mechanism. US Nuclear Regulatory Commission Report, NUREG/CR-0617.

Hewitt, G.F., 1995. In search of two-phase flow. In: 30th US National Heat Transfer Conference, Portland, Oregon.

Jones, L.O., Whitaker, S., 1966. An experimental study of falling liquid films. AIChE J. 12, 525–529.

Joo, S.W., Davis, S.H., Bankoff, S.G., 1991. Long-wave instabilities of heated falling films: two-dimensional theory of uniform layers. J. Fluid Mech. 230, 117–146.

Kapitza, P.L., 1948. Wave flow of thin viscous liquid films. Zh. Teor. Fiz. 18, 3–28.

Kapitza, P.L., Kapitza, S.P., 1949. Wave flow of thin viscous liquid films. Zh. Teor. Fiz. 19, 105–120.

Lee, S.C., Bankoff, S.G., 1984. Parametric effects on the onset of flooding in flat-plate geometries. Int. J. Heat Mass Transfer 27, 1691–1700.

Lee, J.J., Mei, C.C., 1996. Stationary waves on an inclined sheet of viscous fluid at high Reynolds and moderate Weber numbers. J. Fluid Mech. 307, 191–229.

Liu, J., Paul, J.D., Gollub, J.P., 1993. Measurements of the primary instabilities of film flow. J. Fluid Mech. 250, 69–101.

Maron, D.M., Dukler, A.E., 1984. Flooding and upward film flow in vertical tubes – II. Speculations on film flow mechanisms.. Int. J. Multiphase Flow 10, 599–621.

McQuillan, K.W., Whalley, P.B., 1985. A comparison between flooding correlations and experimental flooding data for gas–liquid flow in vertical circular tubes. Chem. Eng. Sci. 40, 1425–1440.

Miles, J.W., 1957. On the generation of surface waves by shear flows. J. Fluid Mech. 3, 185–204.

Nusselt, W., 1916. Die Oberflächenkondensation des Wasserdampfes. Teil I, II. Z. VDI 27 (28), 569–576.

Pushkina, O.L., Sorokin, Y.L., 1969. Breakdown of liquid film motion in vertical tubes. Heat Transfer Soviet Res. 1, 56–64.

Semenov, P.A., 1944. The liquid flow of thin layers. Zh. Tehn. Fiz. 14, 427–437.

Sudo, Y., 1996. Mechanism and effects of predominant parameters regarding limitation of falling water in vertical counter-current two-phase flow. J. Heat Transfer (Trans. ASME) 118, 715–724.

Sudo, Y., Usui, T., Kaminaga, M., 1991. Experimental study of falling water limitation under a counter-current flow in a vertical rectangular channel (1-st report, effect of flow channel configuration and introduction of CCFL correlation). JSME Int. J., Series II 34, 169–174.

Tien, C.L., Liu, C.P., 1979. Studies on vertical two phase countercurrent flooding. Electric Power Research Institute Report, NP-984.

Trifonov, Y.Y., 2008. Wavy film flow down a vertical plate: comparisons between the integral approaches results and the full-scale computations. J. Eng. Thermophys. 17, 30–52.

Vlachos, N.A., Paras, S.V., Mouza, A.A., Karabelas, A.J., 2001. Visual observations of flooding in narrow rectangular channels. Int. J. Multiphase Flow 27, 1415–1430.

Wallis, G.B., Kuo, J.T., 1976. The behaviour of gas–liquid interfaces in vertical tubes. Int. J. Multiphase Flow 2, 521–536.

Zapke, A., Kröger, D.G., 2000a. Counter-current gas–liquid flow in inclined and vertical ducts – I: flow patterns, pressure drop characteristics and flooding. Int. J. Multiphase Flow 26, 1439–1455.

Zapke, A., Kröger, D.G., 2000b. Counter-current gas–liquid flow in inclined and vertical ducts – II: the validity of the Froude-Ohnesorge number correlation for flooding. Int. J. Multiphase Flow 26, 1457–1468.